IMPACT OF Mg ON DIVERSE PROPERTIES OF EUTECTIC AI - SI AUTOMOTIVE ALLOY

Mohammad Salim Kaiser

Innovation Centre
International University of Business Agriculture and Technology
Dhaka-1230, Bangladesh, dkaiser.res@iubat.edu

Received 16 August 2024 Accepted 24 February 2025

DOI: 10.59957/jctm.v60.i3.2025.14

ABSTRACT

Magnesium is an important element for alloying in the composition of Al - Si automotive alloy to enhance mechanical properties and ensure optimum performance. A systematic investigation has been carried out to observe its effect on various properties of this alloy. Investigations include age hardening, thermal conductivity, tensile, wear, corrosion, fracture as well as microstructural properties by developing two Al - Si automotive alloys with and without 0.5 wt. % Mg. Experimental results confirm that both alloys improve its strength during thermal ageing treatment through development of clusters and GP zones alongside metastable phases and maximum can be achieved at around 200°C for 150 min. Addition of Mg provide the different Mg-rich precipitates resulting the better strength. Mg addition in this level improves hardness but reduces the thermal conductivity of automotive alloys by approximately 15 %. Again, the tensile strength improved significantly with a reduction in ductility by 20 % mutually. These Mg - rich intermetallic precipitates improve wear properties by 30 % in dry sliding conditions but suffer 60 % in corrosive environments. Once exposed to an acidic environment, the corrosion rate is elevated by 50 %. Microstructural study confirms plate-like eutectic Si phase and the higher intermetallic created by Mg as coarsen the grain boundary. After being subjected to a temperature of 350°C for 1h, alloys achieve a totally recrystallized state. Fractography of Mg added alloy shows severe breakup occurred at its intermetallic along with a cleavage pattern featuring flat facets indicative of the Al - Si eutectic zone.

<u>Keywords</u>: automotive alloy, corrosive wear, mechanical properties, microstructure, thermal conductivity, T6 heat treatment.

INTRODUCTION

Al-Si alloys have gained widespread recognition for their unparalleled performance in the automotive industry. These alloys are particularly versatile, catering to various requirements based on the Si content present. They are commonly utilized in hypoeutectic, hypereutectic, and eutectic compositions, each offering unique properties and advantages [1, 2]. The hypoeutectic alloys, known for their low silicon content less than 12 wt. %, excel in certain applications requiring specific mechanical properties. On the other hand, hypereutectic alloys containing silicon levels higher than 13 wt. % are favoured for their

enhanced strength and resistance to wear, renders them suitable for demanding automotive elements. Eutectic alloys strike a balance 12 - 13 wt. %, possessing a well-rounded set of properties that make them valuable in diverse automotive applications [3 - 5]. To improve strength or other characteristics as an automotive alloy, small quantities Cu, Ni, Mg, Mn, and Zn are incorporated as minor elements. Furthermore, for grain refinement of the alloys, trace elements such as Zr, Ti, Sc, and Ce are introduced [6 - 9]. It is worth noting that impurities like Fe, Pb, and Sn may originate from the surrounding environment during the melting process, which includes refractory furnaces linings, ladles, reactors, and others.

These impurities play a significant role in influencing the overall properties of the alloys [10]. The addition of an element is widely acknowledged to have a significant effect on boosting the unique characteristics of an alloy, thereby bringing about improvements in its overall properties. This modification not only serves to elevate certain aspects but also leads to notable variations in the alloy's other properties, demonstrating a complex interplay between the different elements within the material. More specifically, the present of Fe in Al - Si cast alloys increased hardness but strongly reduced the mechanical properties such as tensile strength, elongation and fracture toughness due to brittle Fe - rich β-Al5FeSi intermetallic formation by way of a plate-like morphology as briefly discussed in earlier review report [11]. Again, in case of Ni addition, tensile and creep resistance properties of the Al - Si automotive alloy significantly increases through the Al₂Ni intermetallic phase at room and elevated temperatures, while the elongation and thermal conductivity show an opposite trend [12, 13]. Dhakar et al., revealed the complete opposite phenomenon with Zn addition [14]. The addition of Zn reduces the length, diversity and distribution of eutectic Si needles within the Al-Si alloy as the result is reduced tensile strength and increased ductility. Cu and Mg added to Al-Si alloy enhance mechanical properties and enable precipitation hardening. Al-Si-Cu-Mg alloy exhibits high age hardening. Al-Si automotive alloys contain about 2 wt.% Cu and 0.3 - 1 wt.% Mg [15 - 17]. Thermal processes like solutionizing, quenching, and ageing alter the allov's characteristics and ingredient dispersion. Properties of these alloys are dependent on both the duration and temperature at which the aging process occurs. The outstanding thermal conductivity makes the alloy an appropriate alternative to cast iron for making engine components. Al - Si alloy also has the thermomechanical performance required for high engine operating temperatures and increased pressures [18, 19].

Furthermore, it is of utmost importance to thoroughly analyse and evaluate the influence of magnesium on the altered characteristics of aluminium-silicon alloys used in the automotive industry. This diligent investigation is essential for the comprehensive examination and precise identification of the most efficient ways to utilize these alloys for optimal performance. This research involves the preparation of Al - Si automotive alloys, some with 0.5 wt. % Mg and others without, to

thoroughly investigate and assess the potential effects on a wide range of properties displayed by the alloys. Subsequently, a comprehensive evaluation and analysis including hardness, conductivity, tensile strength, wear resistance, corrosion and detailed microstructural examination are meticulously conducted under various ageing conditions. The results obtained from this investigation have the potential to offer valuable perspectives on the adaptability and appropriateness of these alloys in different engineering fields, opening possibilities for future advancements and innovations in the industry.

EXPERIMENTAL

For the formulation of two eutectic Al-Si automotive alloys, aluminium, zinc, magnesium, copper, and nickel of Superior purity standard were utilized, alongside the master alloy Al - 50 wt. % Si. It should be emphasized that one of these was formulated without the inclusion of Mg, while the other alloy contained a Mg of 0.5 wt. %. Other alloving elements and their quantities for both alloys were same and selected depending on the various automotive alloys used. The melting procedure was conducted in a clay-graphite crucible in a pit furnace powered by natural gas, following standard methods. Furnace temperature was closely controlled around 750 ± 10°C. Casting utilized a versatile mild steel mold for shaping products. The cast component, with dimensions of 25 x 150 x 200 mm, was preheated to 250°C before pouring the molten material at around 715°C. Analysis of the alloy composition was done using an optical emission spectrometer, Shimadzu PDA 700, with main components listed in Table 1, excluding negligible elements like Pb, Sn, Zr, Ti, and P.

The cast alloys were treated at 450°C for $12\,\text{h}$, then at 535°C for $2\,\text{h}$ followed by quenching in salt water. They were machined into $20\,\text{x}$ $20\,\text{x}$ 5 mm pieces, aged using different methods in a muffle furnace at $900\pm3^{\circ}\text{C}$, and polished for hardness and conductivity measurements. Micro Vickers Hardness Tester HV-1000DT and electrical conductivity meter type 979 were used for analysis, with thermal conductivity determined by the Wiedemann-Franz law based on the data obtained [20]. The samples were tested for microhardness using a 1 kg load and the knoop indenter for $10\,\text{s}$. A minimum of eleven reading each were taken on the polished sample

Table 1. Compositions based on weight percentage of both samples.

Alloy	Si	Mg	Cu	Ni	Zn	Fe	Al
Alloy 1	12.083	0.021	2.081	0.501	0.960	0.305	Bal
Alloy 2	12.164	0.512	2.146	0.510	0.904	0.294	Bal

for both studies, with the locations varying. The tensile testing was conducted on standard samples using a 4204 model Instron testing machine at a strain rate of 10⁻³ s⁻¹. The dimensions of the tensile test samples were 25 mm gauge length, 6 mm width, and 5 mm thickness. At room temperature following the ASTM guidelines the test was conducted where the averages of five test results were taken. The true stress and true strain curve were plotted based on the value closest to the average of the experimental tensile results.

The solution-treated cast alloys were machined into specimens measuring 14 mm in length and 5 mm in diameter for wear study purposes. These samples underwent age hardening at 200°C for 150 min to reach the peak-aged state. The wear and frictional properties of the tested alloys were analysed according to ASTM standard G99-05, utilizing a pin-on-disc type apparatus [21]. A 309s stainless steel disc, 100 mm semi-diameter, 15 mm thickness was used for example the counter surface material. The disc had a hardness of approximately HRB 85 and a roughness of 0.40 µm. A 20 N load, resulting in a calculated 1.02 MPa interaction pressure, was applied during the wear study. The disc was rotated at 300 rpm, with the pin samples moving a track with a diameter of 49 mm, leading to a sliding velocity of 0.77 m s⁻¹. The distance of sliding was calculated based on the diameter of the track and the rotational speed of the stainless-steel disc. All tests were conducted under ambient conditions of 70 % humidity and a temperature of 22°C. Seven trials were conducted for every data point, and the mean values were considered. The samples underwent testing in dry sliding conditions first, then were exposed to 3.5 % NaCl saline water. In corrosive settings, a drip - type single point lubrication system was consistently maintained at a steady rate of five drops per minute at the contact interface between the specimen and the steel counter plate. Additional information on testing methods and procedures can be found elsewhere [22].

Again, Samples of peak age measuring 55 x 15 x 3 mm were acquired and polished to analyse the corrosion characteristics. Following ethanol cleaning, they were

dried, weighted, and submerged in a corrosive medium containing 0.2 M HCl for varying exposure times of up to 27 days at room temperature. After the designated duration of time exposure in the acidic solution medium, specimens underwent a final weight measurement. Weight-loss measurements were performed on seven samples for each data set and calculated by averaging these values. As stated in the book edited by Marcus, the calculation of the corrosion rate was carried out over the duration of the exposure period [23].

The samples underwent initial polishing with metallographic sandpaper, followed by a final polish with alumina. Standard Keller's reagent was used as the etchant. The samples were etched for approximately 15 sec before microstructures were examined using a trinocular inverted metal microscope model SKU: ME1200TB-10MA. In-depth SEM examination and EDX analysis were carried out on the aged samples using the JEOL JSM-5200 scanning electron microscope, which was equipped with an energy dispersive X - ray analyser (Model: Link AN-10000). Furthermore, the scanning microscope was employed not only to analyse the aged samples but also to investigate the fracture mode of tensile - tested samples and examine the worn surface of alloys subjected to different wear studies.

RESULTS AND DISCUSSION

Microhardness

This work examined two distinct Al-Si automotive alloys: Alloy 1, which was devoid of magnesium, and Alloy 2, which had about 0.5 wt. % of magnesium. Fig. 1 shows the experimental results for those solution-treated alloys from both isochronal and isothermal aging. In the first phase, when alloys are at room temperature, the magnesium addition shows increased hardness. This can be attributed that Mg elements form a supersaturated solid solution in the alloy matrix called solid solution strengthening. Additionally, hard Mg-rich intermetallic precipitates at grain boundaries results the higher hardness [24]. Upon exposure to an isochronal aging

process lasting one hour, a remarkable phenomenon is observed in which double aging peaks with closely similar profiles appeared successively (Fig. 1a). This startling observation has been confirmed by various researchers and this behaviour exemplifies a distinct precipitation pattern exhibited by this alloy, which consists of the following sequence [15, 16, 25]. These mechanisms encompass the formation of GP zones, the precipitation of homogeneous θ'' -Al₂Cu and β'' -Mg₂Si phases, as well as the presence of heterogeneous precipitates such as θ' -Al₂Cu and β' -Mg₂Si intermetallic phases. Additionally, rod or plate-shaped equilibrium phases of θ -Al2Cu and β -Mg2Si also play a significant role. The alloy's strength is primarily attributed to the GP zone and metastable phases in the two distinct aging peaks. Before the coherent precipitation of θ and β-platelets, the alloy achieves its maximum strength. Moreover, various other phases can form, such as β-Al_sFeSi, π-Al_oFeMg₂Si5, and Q-Al_sCu₂Mg₂Si₂, each contributing to the overall strength but to a lesser extent compared to the θ and β phases. The presence of Ni forms ε-Al₂Ni, δ-Al₂CuNi and T-Al₂FeNi phases, which can maintain high thermal stability of the alloy [26]. Yet, Zn existence in the Al matrix enhances the segmentation of Mg, Si and Cu atoms from the matrix into solute clusters, GP zones and β'' precipitates [27]. At the onset of the aging process, a complex interaction unfolds, where fine and numerous GP zones are evenly distributed within the matrix, resulting in a significant increase in strength. As the aging process progresses to its intermediate stage, metastable phases develop, creating a partial coherence with the matrix that effectively impedes dislocation movement, thereby enhancing the material's strength. Importantly, this shift towards metastable phases leads to a considerable dissolution of GP zones, resulting in a marked decrease in their presence within the material. In contrast, the metastable precipitates are too small and have not yet reached adulthood to effectively withstand the movement of dislocation. Because of the aging process, the age-hardening effect of the alloys is diminished during the period between the two peaks of aging, signifying a decrease in the material's ability to strengthen over time. It is evident that, in comparison to another alloy, the Mg - added alloy exhibits a stronger aging response. The Mg linked precipitates like Mg,Si. Q-Al₅Cu₂Mg₈Si₆ and π -Al₉FeMg₃Si₅ are absent as previously mentioned precipitates because it contains

negligible amounts of Mg. In the concluding stage of the aging process, a noticeable decrease in hardness is observed in both alloys. This phenomenon can be attributed to various factors such as recovery, where the material's internal structure starts to stabilize, as well as the coarsening of precipitates within the alloy. Additionally, the inconsistent distribution of these precipitates among the grains contributes to this hardness drop. Moreover, recrystallization, the process of forming new grains within the material, also plays a role in this observed change.

In the event of ageing at 200°C, isothermal ageing leads to an initial increase in the hardness of the alloys due to the formation of high-density GP zones, which exhibit strong strengthening capability. However, as the ageing time progresses, the hardness decreases as a result of GP zone dissolution (Fig. 1b). Upon dissolution of the GP zone, the precipitates undergo growth to reach a stable phase, resulting in a relatively mild strengthening effect. Following these subsequent strengthening effects are observed as associated with nanoscale metastable precipitates [28]. As usual Mg added alloy shows the better strength due to presence of Mg - rich intermetallic. Prolonged exposure to elevated temperatures leads to a reduction in hardness because of over - ageing phenomena related to over ageing effects associated with grain and precipitation coarsening of the alloys. From the combined effects of time and temperature it can be supposed that the optimum precipitation can be formed after ageing at 200°C for an exposure time 150 min where maximum hardness can be achieved.

Thermal conductivity

The changes in Fig. 2, thermal conductivity for two experimental alloys is depicted, illustrating how they evolve over the course of isochronal and isothermal ageing in identical conditions. The conductivity profiles of both alloys exhibit a notable similarity after undergoing treatment with isochronal ageing (Fig. 2a). When comparing the conductivity curves, both alloys show similar thermal behaviour during ageing. Initially, thermal conductivity decreases slowly, then increases, decreases again with ageing temperature, and finally sharply jumps beyond 200°C. It is interesting to observe that in the realm of alloys, the level of conductivity is found to have a reciprocal relationship with the material's hardness. This means that as the hardness of

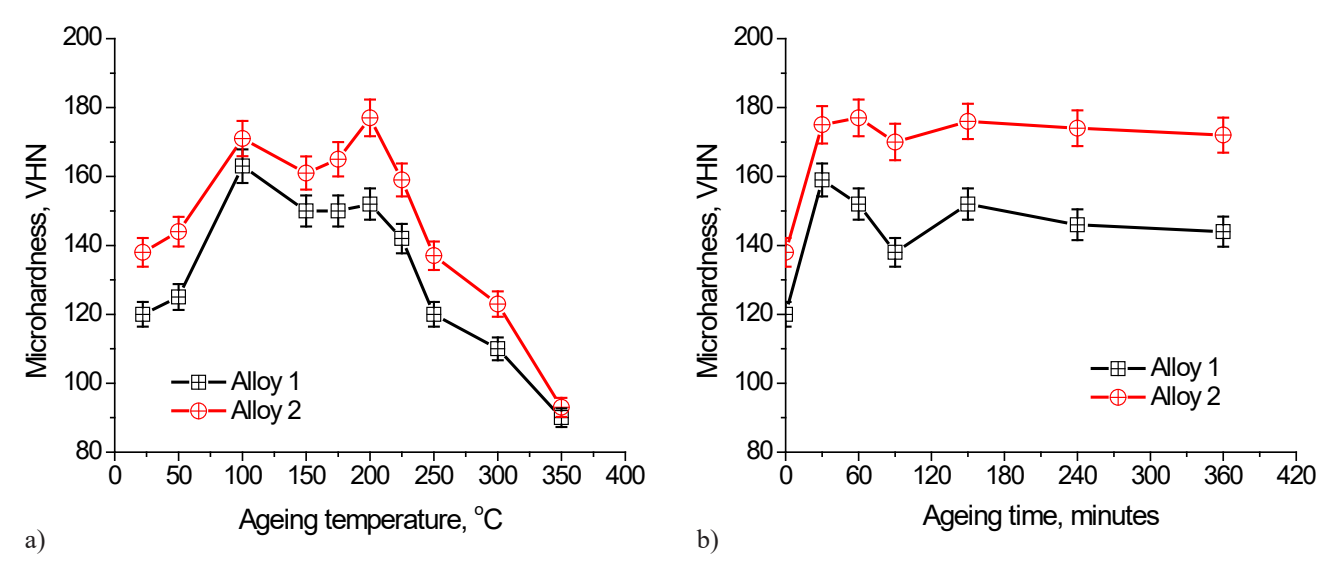


Fig. 1. Characteristics of microhardness for with or without Mg added Al-Si automotive alloys during (a) isochronal ageing and (b) isothermal ageing.

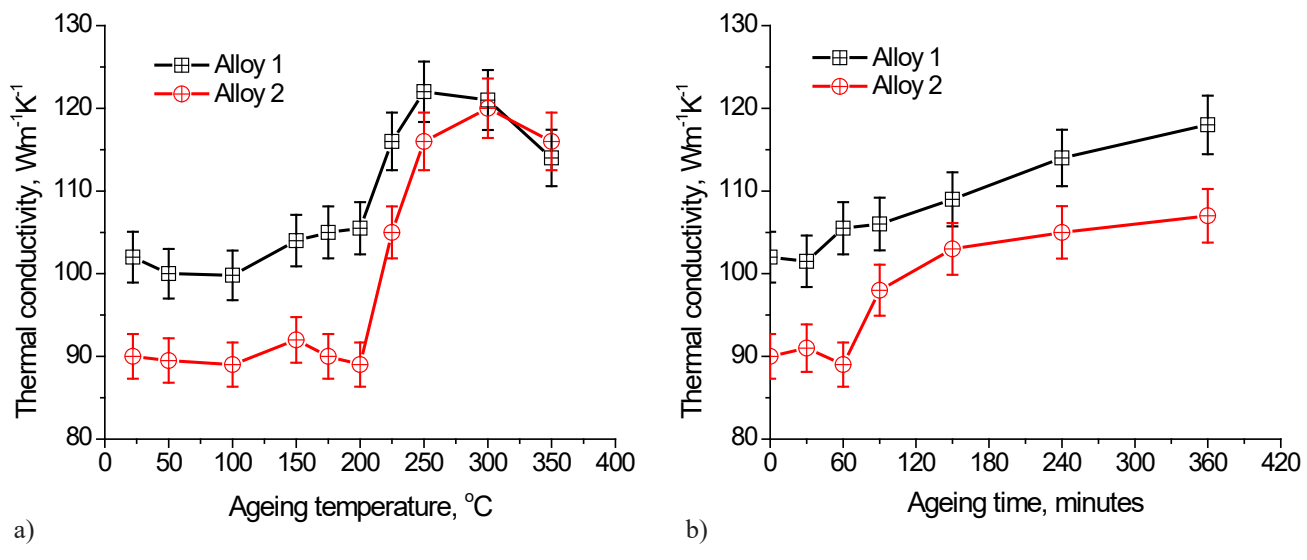


Fig. 2. Characteristics of thermal conductivity for with or without Mg added Al-Si automotive alloys during (a) isochronal ageing and (b) isothermal ageing.

an alloy increases, its conductivity tends to decrease, and vice versa. The first one decrease in conductivity is connected to the creation of the GP zone. The second one, strain recovery due to casting and GP zone dissolution results in increase in conductivity. Again, decreases of conductivity with ageing temperature is for the metastable phase formation of the alloys. The steep jumps up of conductivity of the alloys at the final stage is due to dissolution of metastable phases and the precipitation coarsening which already formed in the matrix [10]. The conductivity of the alloy with Mg

demonstrates the lower since the formation of additional Mg-rich intermetallic which boost the scattering of electrons and phonons as well as solid solution distorts the lattice of the Al matrix and reduces the thermal transportation of electrons.

Following exposure to isothermal aging at 200°C for different durations, the average conductivity values are depicted in Fig. 2b. It is important to highlight that both alloys show a similar overall pattern of conductivity enhancement over time; however, the degree of enhancement varies between the two materials.

However, at the initial stage of ageing around at two hours some fluctuating nature in conductivity of the alloys is noted. There are two things are related with this up down values of conductivity. It is already point out that GP zone and different precipitation formation reduces the conductivity of the alloys and stress reliving, and recovery increase the conductivity of the alloys [29]. The graph illustrates the cumulative findings of the study. As the ageing time increases, the rise in conductivity is closely associated with the precipitation and grain coarsening of the alloys. Fine precipitates make the alloys defect which hinder the electron movement and coarsen precipitates losses the efficiency hence the lower and higher conductivity [30].

Tensile properties

After being subjected to a temperature of 200°C for 150 min, the alloys reached their peak-aged condition, and a tensile test was performed at a strain rate of 10⁻³ s⁻¹. The true stress and true strain curves of both alloys, as shown in Fig. 3, indicate some disparity between them. The automotive alloy, which does not contain Mg, exhibits lower strength and higher elongation percentages. It also displays relatively higher ductility, resulting in a higher slope of true stress-strain curve compared to the Mg-containing alloy. The true stress-strain curves for the Mg-added alloy are more vertical in nature, which can be attributed to dislocation theory [31]. In the peak-aged condition, the alloys contain the highest fraction of fine precipitates. Additionally, during the ageing process, a greater amount of Mg - rich fine precipitates form, creating an additional barrier to dislocation movement. As a result, the Mg - added alloy demonstrates higher tensile strength, lower elongation percentages, and a relatively lower slope of the curve [32, 33].

Wear behaviour

Research has been carried out for investigation the impact of magnesium on wear performance of the automotive alloy in both dry and corrosive sliding environments. Based on the experimental result wear rates and frictional coefficient are plotted against the sliding distance in Figs. 4 and 5. All the cases the samples are tested at their peak aged state, which involves aging at 200°C for 150 min and the sliding velocity and pressure are assumed to be 0.77 m/s and 1.02 MPa respectively. The graphical representation in Fig. 4a clearly displays

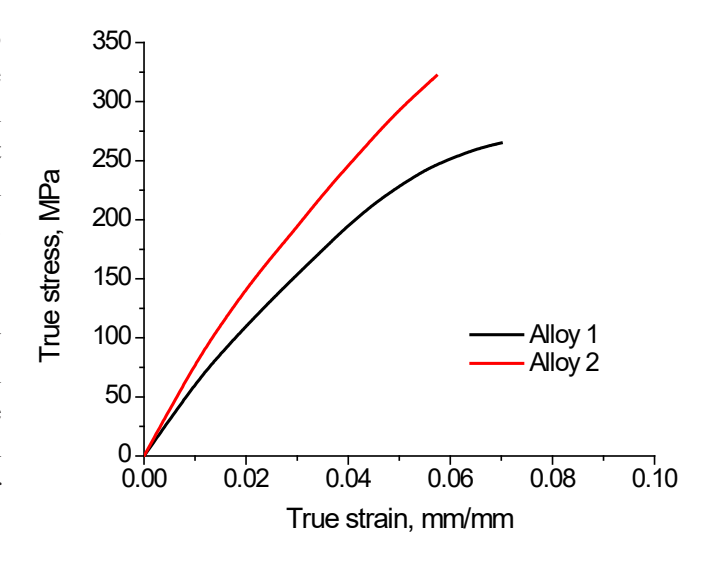


Fig. 3. Discrepancies in the true stress and true strain curves of the two alloys in their peak - aged state.

the wear rate in relation to the sliding distance for both Al-Si alloys under dry sliding conditions. The observed data unambiguously indicates that the inclusion of magnesium led to improved wear properties with a wear rate reduction owing to the formation of various Mg-rich intermetallic compounds, Al, CuMg, Mg, Si, Al₅Cu₂Mg₇Si₇, Al₈Mg₃FeSi₆, Mg(ZnCuAl)₂, thus significantly influencing the overall hardness of the alloys. According to Archard's theory, the wear rate of harder alloy is always lower under dry sliding conditions [34]. These hard particles in the matrix have a higher load - carrying capacity, therefore improving adhesion resistance of the alloy and protecting the matrix from the counter face during the sliding process. It is evident from the figure that as the sliding distance increases, the wear rate also increases in both alloys. The increasing phenomenon of wear rate is associated with process of material softening. Prolonged close contact among two mating surfaces generates heat through pressure and friction resulting in softens the alloy material. So, the weak alloy matrix makes it easy to damage [35]. This tendency is lower for Mg added alloy for its thermally stable precipitates.

When exposed to a corrosive environment such as a 3.5 % NaCl solution, the wear rate shows fully different in nature (Fig. 4b). Higher wear rates are found for Mg added alloy. As previously discussed, Mg provides a strengthening mechanism protecting the surface from

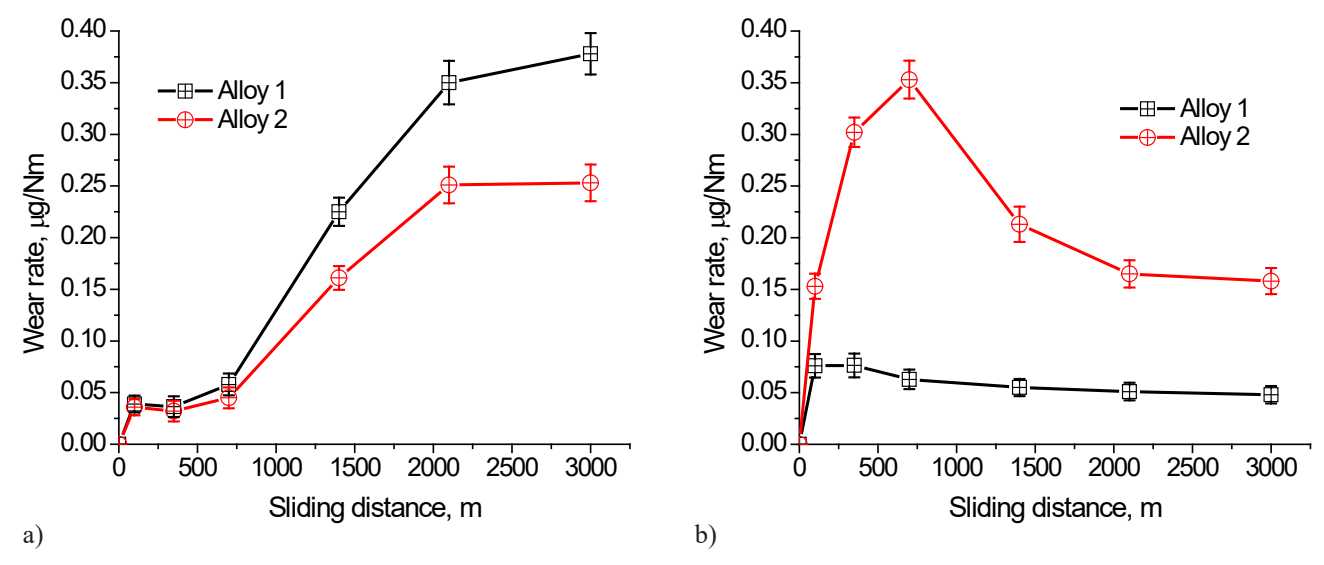


Fig. 4. Wear rate variation of both alloys subjected to (a) dry sliding and (b) corrosive environments under 1.02 MPa pressure and 0.77 m s⁻¹ sliding velocity.

damage, which does not function well as the β-Al₃Mg₂ phase present in the alloys preferentially attacked by corrosive environments [36]. Again, the presence of the MgAlCu phase in the alloy accelerates the corrosion as it acts as a galvanic cathode [37]. Besides, a trace amount of Zn, which enters the alloy matrix as an impurity, often forms Mg(ZnCuAl)₂, which engenders preferential dissolution or dissolution of the precipitate [38]. Besides, there are strong corrosive agents like chlorides present in sodium chloride water which are involved in further loss of material through corrosion reaction, which explains the higher rate of corrosion in these environments when the Mg content is higher [39, 40].

The coefficient of friction starts at a low value and subsequently rises as the sliding distance increases, as depicted in Fig. 5a. The initial low frictional coefficient is attributed to the interaction between the oxide layers adhered to the specimen and the disc material. As the sliding distance increases, the coefficient of friction escalates due to the cracking and removal of the surface oxide layer, resulting in metal-to-metal contact and an increase in frictional coefficient. Interface temperature increases with the increment in sliding distance that may promote the surface oxidation and reduce the direct metal contact hence there is slight decline in frictional coefficient [41]. This tendency is greater for the Mg added alloy because of the higher oxide formation through this element. The Mg free alloy exhibits a

notably higher coefficient of friction compared to the Mg added alloy under dry sliding conditions. This finding aligns well with the observed microhardness values of the respective alloys. Discrepancies in the level of localized plastic deformation at the actual contact regions could contribute to variations in the friction coefficient. The Mg added alloy has exhibited lower friction as they are harder and undergo less plastic deformation [42].

Under corrosive sliding environment the hardness of alloy upon addition of Mg does not showy because of it is affected by corrosive environment and the corrosive product are removed simultaneously as well as not too hard as before as dry sliding condition (Fig. 5b). The friction coefficient of two alloys is higher in a dry environment compared to a corrosive environment. The cause of this friction reduction is the "Sealing Effect", which reduces the roughness of the surfaces during sliding in contact [43].

Corrosion behaviour

The corrosion rates, measured in mm per year, were determined through weight-loss experiments. These rates are illustrated in Fig. 6 for the two Al - Si alloys tested over a period of 27 days in 0.2 M HCl solutions. The figure displays typical corrosion profiles seen in most passivating metals when exposed to corrosive conditions [23, 44]. Each alloy's corrosion

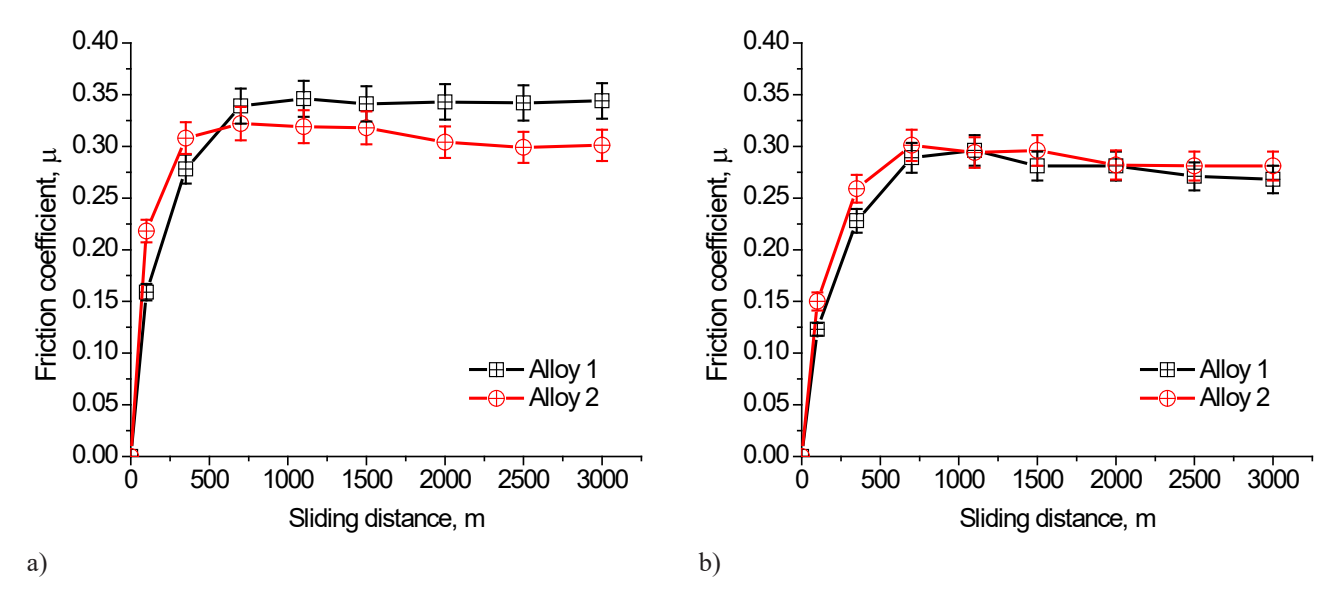


Fig. 5. Friction coefficient variation of both alloys subjected to (a) dry sliding and (b) corrosive environments under 1.02 MPa pressure and 0.77 m s⁻¹ sliding velocity.

profile exhibits a rapid rise in corrosion rate at the beginning, followed by a peak value representing the active dissolution phase. Afterward, the corrosion rate diminishes gradually as passivation takes place, attributed to the development of oxide on the surface of the metal. With increased duration of exposure, the buildup of corrosion byproducts forms a protective layer and consistent corrosion rate, occurs. The findings of higher corrosion rate related to the Mg addition can be attributed to the intense ionic attack of chloride, causing disruption of protective films on the exterior of the metal. Again, inter-granular corrosion and localized pitting occurs due to the presence of electrochemically active magnesium aluminite phase along the grain boundaries in different sensitized conditions [45].

Optical micrographs

In Fig. 7, the optical micrograph of both alloys is presented to observe the effect of Mg under different ageing treatments. While the experimental automotive alloys are subjected to solutioning at 535°C for 2 h and then undergo ageing treatment at 200°C for 150 min to achieve the peak aged condition, as well as at 350°C for 60 min to achieve the over aged condition. At the pinnacle of aging, the alloys maintain their grain orientation without alteration. Only stress relief and precipitation may result from this heat treatment

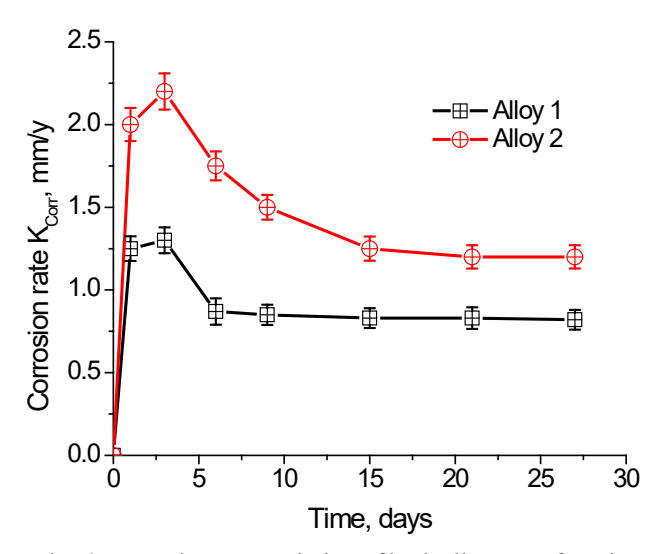


Fig. 6. Corrosion rate variation of both alloys as a function of immersion time exposed during 27 days in 0.2 M HCl solutions.

regimen. The microstructure of the base Alloy 1, without Mg added Al - Si automotive alloy consists of mainly primary α-Al, eutectic Si and Al₂Cu. Additionally, the Fe-rich phase is predominantly present in the form of Al₅FeSi (Fig. 7a). With addition of Mg in Alloy 2, the Al₅FeSi phase vanishes, while the Al₈Mg₃FeSi₆ phase and the Mg₂Si phase emerge in the microstructure (Fig. 7b).

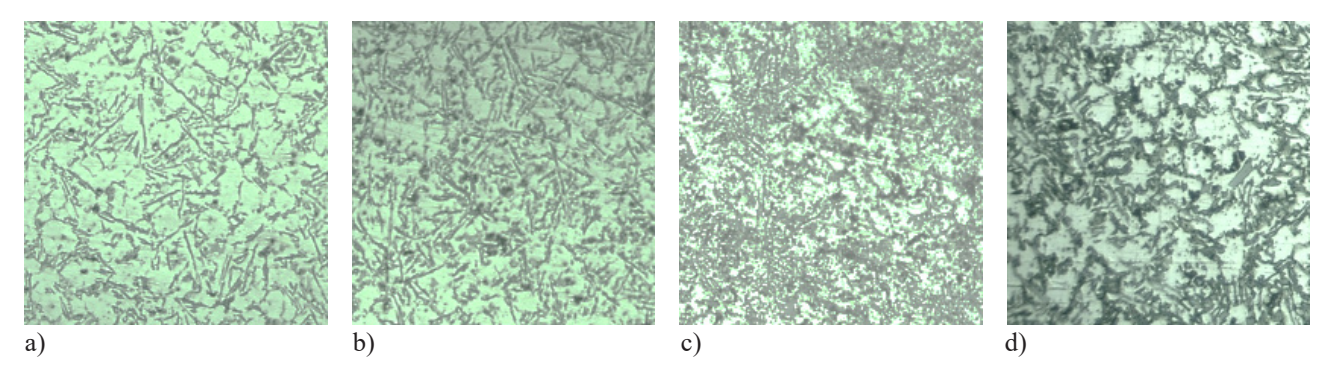


Fig. 7. Microstructure of (a) Alloy 1, (b) Alloy 2 aged at 200°C for 150 min and (c) Alloy 1, (d) Alloy 2 aged at 350°C for 60 min.

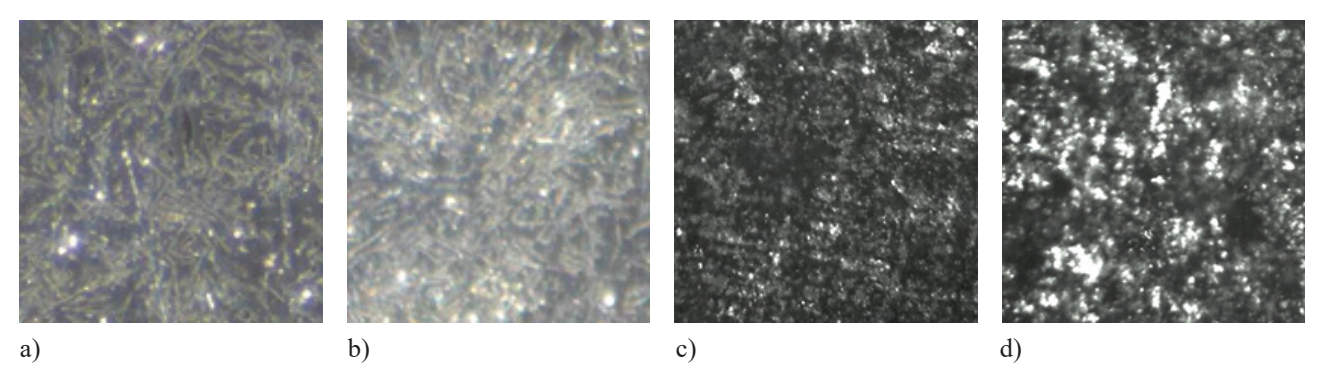


Fig. 8. Microstructure of polished Al-Si alloys before (a) Alloy 1, (b) Alloy 2 and after corrosion (c) Alloy 1, (d) Alloy 2 in 0.2 M HCl environmental for 27 days.

Due to higher amount of different precipitates forms through the Mg as a result the microstructure background is relatively dense.

After undergoing an aging process at 350°C for a duration of 1 h equiaxed grains are observed for both alloys where the backgrounds of the microstructure are not too clear as the microstructure of the prior state are displayed (Figs. 7c and 7d). At this temperature applied for 1 h, the dendrites give the impression of dissolution in addition to intermetallic coarsening occurred which homogeneously distributed into the alloy matrix [46]. Accordingly, microstructures of two alloys turn to equiaxed grains. In case of Mg added alloy higher second phase are clearly seen into the alloy.

Depicted in Fig. 8 are the optical micrographs of the highly polished surface of both alloys before and after being immersed in 0.2 M HCl solutions for a period of 27 days. Prior to corrosion test, both alloys exhibit smooth surfaces with no signs of plastic deformation. Some irregularities are visible due to the polishing

process. The polished microstructure does not provide meaningful information without etching. As previously mentioned, these alloys are composed of an Al - rich dendritic matrix, α -Al phase, and a eutectic combination in the interdendritic zone. Consequently, the polished surfaces displaying diverse shades owing to the varying concentrations of alloying elements present in the alloys. It is evident that the differences are attributed to the addition of Mg, which alters the dendrite structure and forms various intermetallics [47].

Upon extraction of the specimens from the acidic solution, a significant level of corrosion was detected. These findings primarily suggested that the pit formation on the surface is prominent, what is due to the surface attack by the aggressive chloride ions [48]. The microstructure of Mg added corroded samples the surfaces show the higher degradation of the alloy, Mg-rich intermetallic especially magnesium aluminite with uniform attack of hydroxide ion on the surface of metal [45].

SEM observation

Along with the corresponding spectra from the scanning electron microscope equipped with energy-dispersive X - ray spectroscopy to comply with the optical images of the alloys at its peak aged condition are kept being shown in Fig. 9. Base Alloy 1 confirms the α -Al phase and elongated needle-like eutectic silicon

structures as well as various intermetallic particles in the microstructure (Fig. 9a). But the intermetallic linked with Mg are almost absent. The corresponding EDX composition is 44.77 % Al, 51.88 % Si, 1.18 % Cu, 0.07 % Mg, 1.10 % Zn and 0.25 % Ni in 0.72 wt. % Fe and 0.03 % Mn. Similarly, Mg added Alloy 2 confirms different Mg-rich intermetallic along with $\alpha\text{-Al}$, needle -

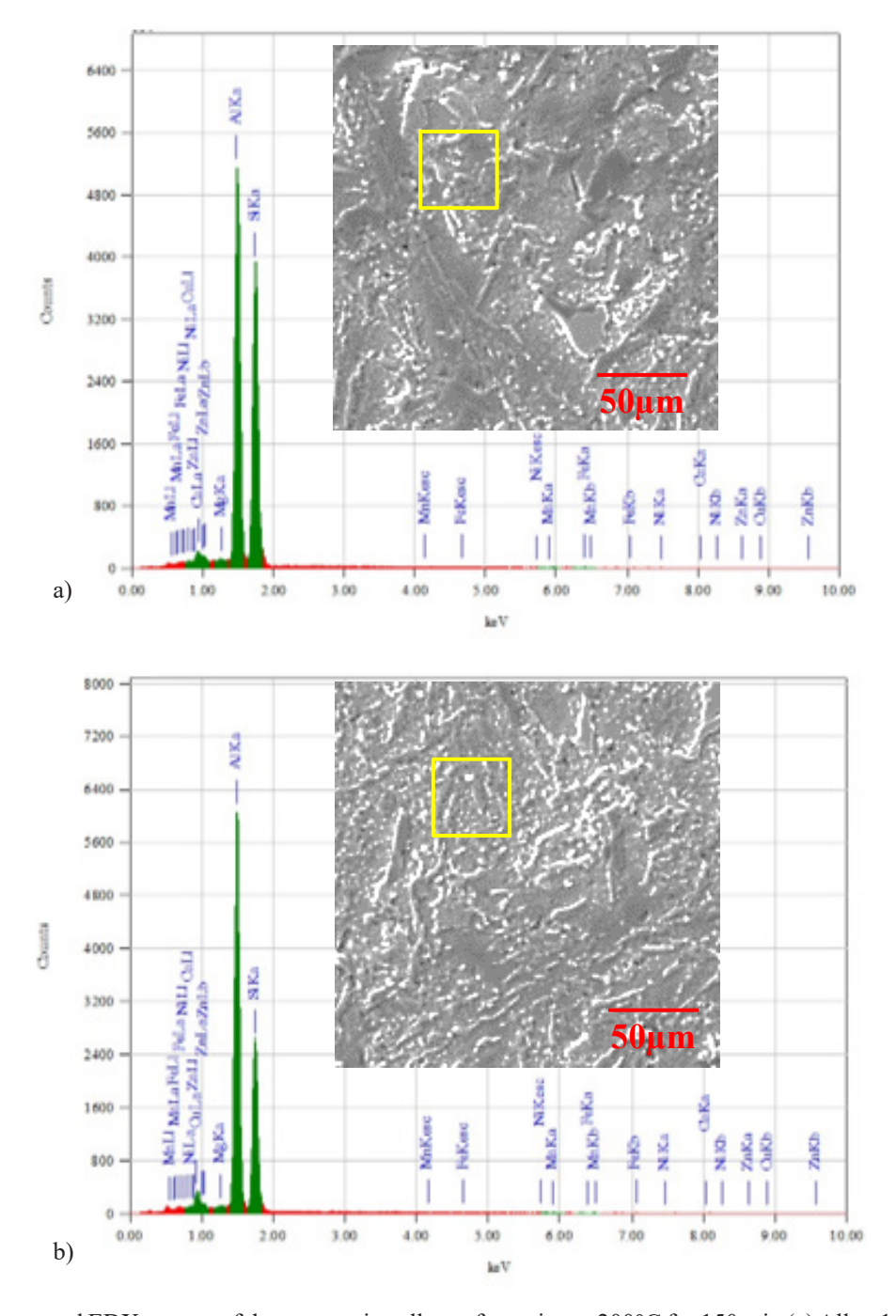


Fig. 9. SEM images and EDX spectra of the automotive alloys after aging at 200°C for 150 min (a) Alloy 1 and (b) Alloy 2.

like eutectic Si and other intermetallic (Fig. 9b). EDX specifies 56.64 % Al, 39.58 % Si, 2.01 % Cu, 0.24 % Mg, 0.86 % Zn and 0.58 % Ni in 0.05 wt. % Fe, 0.04 % Mn in this case. It is important to recognize that the reduction in the size of eutectic silicon is a direct result of the creation of supplementary Mg₂Si within the alloy matrix [49]. As a result of several silicon-rich intermetallic compounds formation, the chemical analysis indicates reduced levels

of silicon within the specific region as illustrated by EDX results obtained from the SEM.

Fig. 10 displays the SEM micrograph of worn surfaces of alloys with and without the addition of Mg after undergoing 3000 meters of wear testing under both dry and 3.5% NaCl conditions. The testing conditions included an applied pressure of 1.02 MPa and a sliding velocity of 0.77 m s⁻¹. The figure also features the

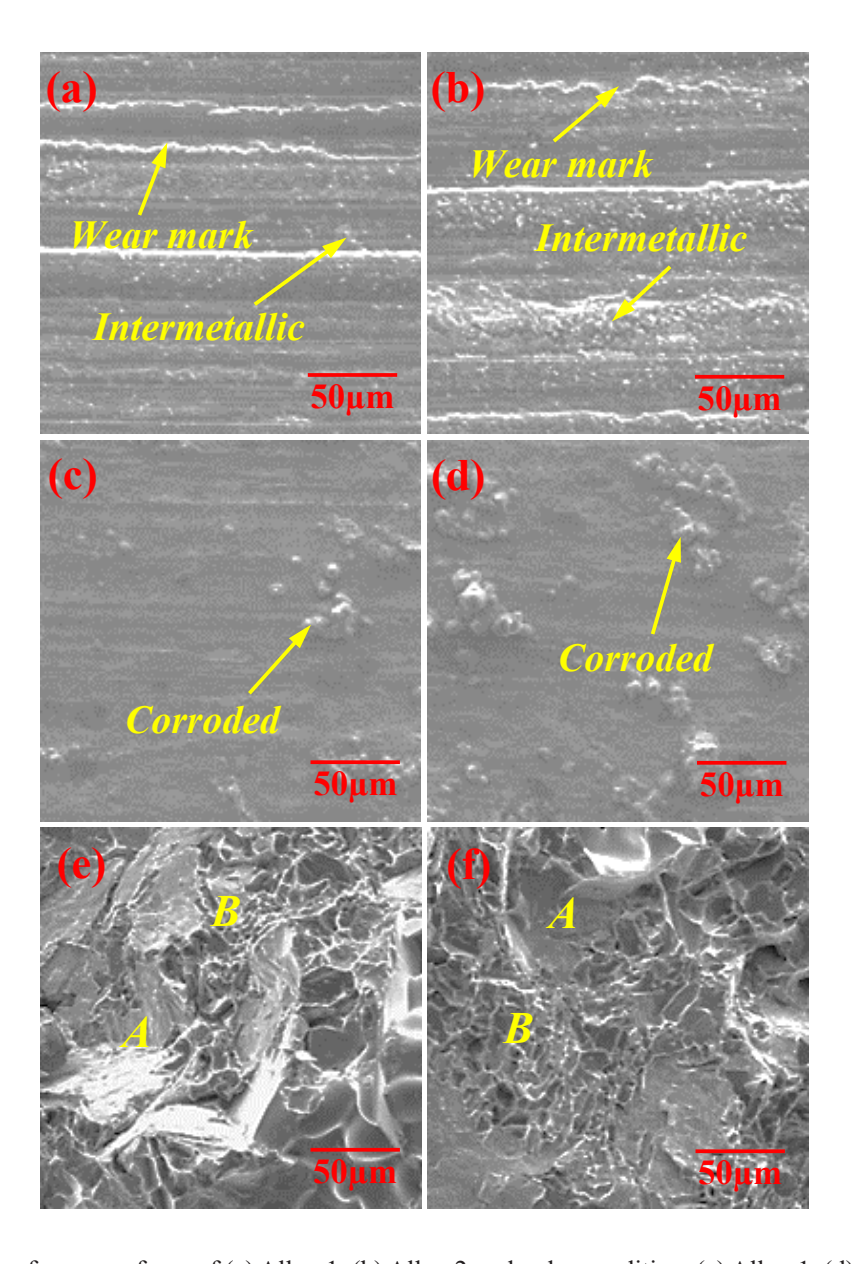


Fig. 10. SEM images of worn surfaces of (a) Alloy 1, (b) Alloy 2 under dry condition, (c) Alloy 1, (d) Alloy 2 under 3.5% NaCl solution environment after being subjected to 3000 m of sliding and tensile fracture surfaces of (e) Alloy 1, (f) Alloy 2.

fracture morphologies of both alloys for comparative analysis and investigation. The samples underwent the standard solution treatment, followed by aging at their peak-aged condition and were subsequently subjected to tensile testing at a strain rate of 10⁻³ s⁻¹. As Mg added Alloy 2 shows the best wear performance in case of dry sliding environment, SEM observations are made between this and Mg free Alloy 1 (Figs. 10a and 10b). The figure depicts that the surfaces under dry condition are mostly damaged from abrasive wear with oxides, which is dictated by the haphazard crevices and numerous deep marks that are distributed all over. On the other hand, small, grooved cracks, and dislodged material, demonstrating combination of mild and the flat rough tracks filled with oxidized substances, are visible on surfaces of Mg added alloy. This proves that it has better wear resistance. The reason is, higher level of Mg, Si as well as Mg - rich intermetallic, which strengthen and harden the alloys. The examination of the deteriorated surfaces of the two alloys in the corrosive wear trial carried out under the same circumstances indicates the existence of corrosive substances on each surface. Upon examining the surface imagery, it becomes evident that the alloy containing Mg exhibits a markedly elevated degree of corrosion when compared to the magnesium-free alloy, as illustrated in Figs. 10c and 10d. It has been previously established that the Mg originating from aluminate contributes to the susceptibility of stress corrosion cracking, a vulnerability that intensifies when exposed to corrosive environments [50, 51]. Two typical fracture characteristics in this automotive alloy are observed "A" and "B" in both fracture surfaces (Figs. 10e and 10f). In the absence of Mg Alloy 1, a cleavage pattern displaying flat facets labelled as "A" is observed, representing the Al - Si eutectic zone. Within these flat regions, the Si platelet may detach from the Al matrix, resulting in a terrace with a smooth facet. These facets are likely a consequence of the fracture of brittle Si phase crystals [52, 53]. Conversely, broken intermetallic compounds may be present in this micrograph, particularly in area "B". The higher intermetallic content introduced by Alloy 2 containing Mg leads to a more pronounced breakup at these intermetallic sites, accompanied by reduced cleavage facets. This means that the stress field of the main crack broke up the intermetallic due to their poor deformation properties [54].

CONCLUSIONS

By conducting a thorough experiment, it is possible to derive the following conclusions regarding the influence of Mg on the specific characteristics of automotive Al - Si alloy.

Aged Al-Si automotive alloys have a unique hardness profile with two distinct peaks due to the aging process, which involves the formation of various phases like GP zones and metastable phases. Key strengthening intermetallic compounds include θ -Al₂Cu, β -Mg₂Si, ϵ -Al₃Ni, δ -Al₃CuNi, and Q-Al₅Cu₂Mg₈Si₆, with magnesium-related compounds playing a crucial role in enhancing properties. Optimal hardness requires precise aging at around 200°C for approximately 150 min.

The thermal conductivity of the alloy is reduced by the addition of Mg, as it leads to the creation of Mg - linked intermetallic compounds that hinder the heat transport of electrons and phonons. However, the reduction of conductivity during ageing due to the formation of precipitates in both GP zones and metastable phases. Additionally, the thermal conductivity increases because of the relief of internal stress from casting, dissolution of metastable phases, and coarsening of precipitates within the alloy.

Magnesium inclusion controlled to a drop in the wear rate then friction coefficient because of the creation of various hard Mg-rich intermetallic compounds which protect the matrix from the counter face during the sliding process. In case of 3.5 % NaCl corrosive environment higher wear rates are found as the β -Al₃Mg₂ phase present in the alloys preferentially attacked by corrosive environments. Consequently, worn surfaces of the Mg - added alloy exhibit comparatively reduced abrasive wear and plastic deformation under dry sliding conditions. In a corrosive environment, the Mg-containing alloy demonstrates significantly greater corrosion compared to the magnesium-free alloy.

The presence of Mg within the alloy leads to an escalation of corrosion rate under acidic environment, associated with the aggressive effect of chloride ions, which leads to degradation of the protective oxide layer present on the alloy surface. Furthermore, intergranular corrosion and localized pitting resulted from electrochemically active magnesium aluminate phases along grain boundaries under different sensitized conditions.

SEM micrographs demonstrate the reduced size of eutectic silicon of Mg added alloy that is a direct result of supplementary Mg₂Si intermetallic formation within the alloy matrix. Under tensile loading fracture surfaces exhibit a cleavage pattern characterized by flat facets that correspond to the Al - Si eutectic zone. Conversely, certain fractured intermetallic may also be observed within the micrograph of the Mg-inclusive alloy.

Acknowledgements

The author is grateful to the honourable Treasurer for the significant support and encouragement provided in advancing research activities at IUBAT, Dhaka.

Author's contribution: All the research projects detailed in the manuscript have been carried out by the effords of M.S. Kaiser.

REFERENCES

- F.C.R. Hernandez, J.M.H. Ramírez, R. Mackay, Al-Si Alloys Automotive, Aeronautical, and Aerospace Applications, Springer International Publishing AG, Cham, Switzerland, 2017.
- S.S. Dash, D. Chen, A Review on Processing-Microstructure-Property Relationships of Al-Si Alloys: Recent Advances in Deformation Behavior, Metals., 13, 609, 2023, 1-64.
- A.A. Razin, D.S. Ahammed, A.A. Khan, M.S. Kaiser, Thermophysical properties of hypoeutectic, eutectic and hypereutectic Al-Si automotive alloys under ageing treatment, J. Chem. Technol. Metall., 59, 3, 2024, 673-682.
- D.S. Ahammed, A.A. Razin, A.A. Khan, M.S. Kaiser, Mechanical Properties of Hypoeutectic, Eutectic, and Hypereutectic Al-Si Automotive Alloys under Ageing Treatment, Eng. Rev., 44, 1, 2024, 1-13.
- A.A. Khan, A.K. Hossain, M.S. Kaiser, Impact of Deep Seawater on the Electrochemical Corrosion Performance of Hypoeutectic, Eutectic and Hypereutectic Al-Si Automotive Alloys, Int. J. Automot. Mech. Eng., 20, 3, 2023, 10798-10807.
- 6. H. Kaya, A. Aker, Effect of alloying elements and growth rates on microstructure and mechanical properties in the directionally solidified Al-Si-X alloys, J. Alloys Compd., 694,2017, 145-154.

- 7. M.S. Kaiser, M.R. Basher, A.S.W. Kurny, Effect of scandium on microstructure and mechanical properties of cast Al-Si-Mg alloy, J. Mater. Eng. Perform., 21, 7, 2012, 1504-1508.
- 8. L. Xiao, H. Yu, Y. Qin, G. Liu, Z. Peng, X. Tu, H. Su, Y. Xiao, Q. Zhong, S. Wang, Z. Cai, X. Zhao, Microstructure and Mechanical Properties of Cast Al-Si-Cu-Mg-Ni-Cr Alloys: Effects of Time and Temperature on Two-Stage Solution Treatment and Ageing, Materials (Basel), 16, 7, 2023, 1-16.
- 9. S.K. Shaha, F. Czerwinski, W. Kasprzak, J. Friedman, D.L. Chen, Ageing characteristics and high-temperature tensile properties of Al-Si-Cu-Mg alloys with micro-additions of Cr, Ti, V and Zr, Mater. Sci. Eng. A, 652, 2016, 353-364.
- 10. Y.N. Mansurov, J.U. Rakhmonov, N.V. Letyagin, A.S. Finogeyev, Influence of impurity elements on the casting properties of Al-Mg based alloys, Nonferrous Metals, 1, 1, 2018, 24-29.
- 11. M.S. Kaiser. Role of excessive iron on hyper-eutectic Al-Si automotive alloy: A Review, JMES, 8, 2, 2021, 241-251.
- 12. L. Zuo, B. Ye, J. Feng, H. Zhang, X. Kong, H. Jiang, Effect of ε-Al₃Ni phase on mechanical properties of Al-Si-Cu-Mg-Ni alloys at elevated temperature, Mater. Sci. Eng. A., 772, 138794, 2020, 1-18.
- 13. Y.H. Cho, H.W. Kim, J.M. Lee, M.S. Kim, A new approach to the design of a low Si-added Al–Si casting alloy for optimising thermal conductivity and fluidity, J. Mater. Sci., 50, 2015, 7271-7281.
- 14. P. Dhakar, S. Kumar, S. Manani, A.K. Pradhan, Effect of Zn content on microstructure and properties of hypoeutectic and near-eutectic Al-Si alloys, IOP Conf. Ser. Mater., 1248, 012020, 2022, 1-8.
- 15. P. Zhou, D. Wang, H. Nagaumi, R. Wang, X. Zhang, X. Li, H. Zhang, B. Zhang, Microstructural Evolution and Mechanical Properties of Al-Si-Mg-Cu Cast Alloys with Different Cu Contents, Metals, 13, 98, 2023, 1-13.
- 16. B. Şenyurt, D. Ağaoğulları, N. Akçamlı, Al-Si-Cu-Mg Matrix Composites with Graphene: PM-Based Production, Microstructural, and Mechanical Properties, Adv. Eng. Mater., 26, 2024, 2400046, 1-11.
- 17. C.Y. Jeong, High Temperature Mechanical Properties of AlSiMg(Cu) Alloys for Automotive Cylinder Heads, Mater. Trans., 54, 4, 2013, 588-594.
- 18. D.S. Ahammed, A.A. Khan, A.A. Razin, M.S. Kaiser,

- Impact of under, peak and over-ageing on the wear properties of Si-doped Al-based automotive alloy, Materials Today: Proceedings, 82, 2023, 300-307.
- 19. A.A. Razin, D.S. Ahammed, A.A. Khan, M.S. Kaiser, Dissimilarity of physical and mechanical properties of Al-(0.2–17.9 wt%) Si automotive alloys in under ageing, peak ageing, and over ageing conditions, Materials Today: Proceedings, 82, 2023, 248-254.
- 20. G.V Chester, A. Thellung, The Law of Wiedemann and Franz., Proc. Phys. Soc., 77, 5, 1961, 1005-1013.
- 21.ASTM G99-05, Standard Test Method for Wear Testing with a Pin-on-Disk Apparatus, American Society for Testing and Materials, West Conshohocken, Pennsylvania, USA, 2010.
- 22. A.A. Khan, M.S. Kaiser, Wear properties analysis on Al-based automotive alloy with varied levels of Si in dry, 3.5% NaCl and seawater corrosive environments. Arch. Metall. Mater., 69, 3, 2024, 881-890.
- 23. P. Marcus, Corrosion Mechanisms in Theory and Practice, 3rd Edition, CRC Press, Florida, USA, 2011.
- 24. M.S. Kaiser, A.A. Matin, K.M. Shorowordi, Role of Mg and minor Zr on the wear behavior of 5xxx series Al alloys under different environments, JMEE, 4, 3, 2020, 209-220.
- 25. A.M.A. Mohamed, F.H. Samuel, A Review on the Heat Treatment of Al-Si-Cu/Mg Casting Alloys, IntechOpen, London, UK, 2012.
- 26. L. Xiao, H. Yu, Y. Qin, G. Liu, Z. Peng, X. Tu, H. Su, Y. Xiao, Q. Zhong, S. Wang, Z. Cai, X. Zhao, Microstructure and Mechanical Properties of Cast Al-Si-Cu-Mg-Ni-Cr Alloys: Effects of Time and Temperature on Two-Stage Solution Treatment and Ageing, Materials, 16, 2675, 2023, 1-16.
- 27. S. Zhu, Z. Li, L. Yan, X. Li, S. Huang, H. Yan, Y. Zhang, B. Xiong, Effects of Zn addition on the age hardening behavior and precipitation evolution of an Al-Mg-Si-Cu alloy, Mater. Charact., 145, 2018, 258-267.
- 28. E. Sjolander, S. Seifeddine, The heat treatment of Al-Si-Cu-Mg casting alloys, J Mater Process Technol., 210, 10, 2010, 1249-1259.
- 29. Y. Ma, Y. Huang, X. Zhang, Precipitation thermodynamics and kinetics of the second phase of Al-Zn-Mg-Cu-Sc-Zr-Ti aluminum alloy, J. Mater. Res. Technol., 10, 2021, 445-452.

- 30. T.R. Prabhu, Effects of ageing time on the mechanical and conductivity properties for various round bar diameters of AA 2219 Al alloy, Eng. Sci. Technol. Int. J., 20, 1, 2017, 133-142.
- 31. S.J. Andersen, C.D. Marioara, J. Friis, S. Wenner, R. Holmestad, Precipitates in aluminium alloys, Adv. Phys-X, 3, 1, 2018, 790-813.
- 32. M.R. Shoummo, A.A. Khan, M.S. Kaiser, True stress-strain behavior of Al-based cast automotive alloy under different ageing conditions and the effect of trace Zr, J. Mechanical Eng. Sci. Technol., 6, 2, 2022, 95-106.
- 33. M.S. Kaiser, Tensile and Fracture Behaviour of Sn/Pb Solder Affected Aluminium Subjected to Post-Deformation Ageing, IUBAT Review, 7, 1, 2024, 186-201.
- 34. J.F. Archard, Contact and rubbing of flat surfaces, J. Appl. Phys., 24, 1953, 981-988.
- 35. M.S. Prabhudev, V. Auradi, K. Venkateswarlu, N.H. Siddalingswamy, S.A. Kori, Influence of Cu addition on dry sliding wear behaviour of A356 alloy, Procedia Eng., 97, 2014, 1361-1367.
- 36. Y. Zhu, D.A. Cullen, S. Kar, M.L. Free, L.F. Allard, Evaluation of Al₃Mg₂ Precipitates and Mn-Rich Phase in Aluminum-Magnesium Alloy Based on Scanning Transmission Electron Microscopy Imaging, Metall. Mater. Trans. A., 43, 13, 2012, 4933-4939.
- 37. X.W. Wang, W. Wang, W. Chen, D.M. Chen, Effect of Al addition and heat treatment on the microstructures and corrosion resistance of Mg-Cu alloys, J. Mater. Sci. Technol., 98, 2022, 219-232.
- 38.Q. Meng, G.S. Frankel, Effect of Cu Content on Corrosion Behavior of 7xxx Series Aluminum Alloys, J. Electrochem. Soc., 151, 5, 2004, 271-284.
- 39. H. Ezuber, A.E. Houd, F.E. Shawesh, A study on the corrosion behavior of aluminum alloys in seawater, Mater. Des., 29, 4, 2008, 801-805.
- 40.Z.S. Smialowska, Pitting corrosion of aluminum, Corros. Sci., 41, 9, 1999, 1743-1767.
- 41. M.S. Kaiser, A Comparative Study on Wear Properties of Highly Conductive Materials Commercially Pure Al and Cu, IUBAT Review, 6, 2, 2023, 77-91.
- 42. A.J.W. Moore, W.J.M. Tegart, Relation between friction and hardens, Proc. R. Soc. Lond., Ser. A, Math. Phys. Eng. Sci., 212, 1111, 1952, 452-458.
- 43. B.N.J. Persson, U. Tartaglino, O. Albohr, E. Tosatti,

- Rubber friction on wet and dry road surfaces: The sealing effect, Physical review B, Condensed matter., 71, 3, 2005, 1-8.
- 44. B.A. Omran, A.M.O. Salam, Basic Corrosion Fundamentals, Aspects and Currently Applied Strategies for Corrosion Mitigation, in: A New Era for Microbial Corrosion Mitigation Using Nanotechnology, Adv. Mater. Res. Technol., Cham., Switzerland, 2020.
- 45. V.K. Beura, C. Kale, S. Srinivasan, C.L. Williams, K.N. Solanki, Corrosion behavior of a dynamically deformed Al-Mg alloy, Electrochimica Acta, 354, 136695, 2020, 1-27.
- 46. Y. Wu, C. Zhao, Y. Han, J. Sun, Z. Li, G. Zu, W. Zhu, X. Ran, A new SLM-manufactured AlSi alloy with excellent room and elevated-temperature mechanical properties, J. Manuf. Process, 133, 2025, 25-32.
- 47. M.A. Nur, A.A. Khan, S.D. Sharma, M.S. Kaiser, Electrochemical corrosion performance of Si doped Al-based automotive alloy in 0.1 M NaCl solution, J. Electrochem. Sci. Eng., 12, 3, 2022, 565-576.
- 48.M. Liu, Y. Jin, C. Zhang, C. Leygraf, L. Wen, Density-functional theory investigation of Al pitting corrosion in electrolyte containing chloride ions,

- Appl. Surf. Sci. B., 357, 2015, 2028-2038.
- 49.B. Jiang, S. Xu, H.Y. Xu, M.L. Hu, Y.J. He, Z.S. Ji, Effect of Mg addition on microstructure and mechanical properties of Al-Si-Cu-Fe alloy with squeeze casting, Mater. Res. Express., 7, 1, 2019, 1-9.
- 50. G.R. Argade, N. Kumar, R.S. Mishra, Stress corrosion cracking susceptibility of ultrafine grained Al-Mg-Sc alloy, Mater. Sci. Eng. A., 565, 2013, 80-89.
- 51.A.A. Khan, M.S. Kaiser, Wear studies on Al-Si automotive alloy under dry, fresh and used engine oil sliding environments, Research on Engineering Structures and Materials, 9, 1, 2023, 1-18.
- 52. Y. Meng, H. Zhang, X. Li, X. Zhou, H. Mo, L. Wang, J. Fan, Tensile Fracture Behavior of 2A14 Aluminum Alloy Produced by Extrusion Process, Metals, 12, 184, 2022, 1-13.
- 53. D.A. Lados, D. Apelian, J.F. Major, Fatigue Crack Growth Mechanisms at the Microstructure Scale in Al-Si-Mg Cast Alloys: Mechanisms in Regions II and III, Metall. Mater. Trans. A, 37A, 8, 2006, 2405-2418.
- 54. G. Zhang, J. Zhang, B. Li, W. Cal, Characterization of tensile fracture in heavily alloyed Al-Si piston alloy, Prog. Nat. Sci., 21, 5, 2011, 380-385.